Journal of Structural Geology, Vol. 10, No. 7, pp. 673 to 684, 1988
Printed in Great Britain

0191-8141/88 $03.00 + 0.00

Stress estimates and fault history from quartz microstructures

T. G. BLENKINSOP*

Department of Geology, University of Keele, Staffs ST5 5BG, U.K.

and

M. R. DRURY†

Instituut voor Aardwetenschappen, Rijksuniversiteit Utrecht, The Netherlands

(*Received* 7 *September* 1987; *accepted in revised form* 13 *June* 1988)

Abstract—Fault plane structures and microstructures have been examined from a fault in Cambro-Ordovician quartzites exposed on the north coast of the Cantabrian zone, N.W. Spain. Along the fault there is a 2–3 cm wide cataclasite zone bounded by plastically deformed intact quartzite, which is restricted to a few metres from the fault plane. In thin section, the cataclasite consists of angular fragments of quartz in a fine-grained matrix of quartz cement. Cathodoluminescence reveals extensive intra- and transgranular microcracking. Deformation lamellae (D.L.) are widespread in the intact quartzite; electron microscopy shows that they are defined by a banded dislocation substructure.

The microstructures indicate a fault history consisting of plastic deformation restricted to a metre-scale zone, followed by cataclasis and dilational fracture. The early plasticity is interpreted as evidence for the propagation of a process zone.

The D.L. are used as an indicator of power-law-breakdown creep, which occurs above a critical normalized stress, estimated as at least 170 MPa from available data. Dislocation densities also indicate a stress higher than 116 MPa. The process zone as defined by formation of D.L. is modelled using fracture mechanics theory. For the likely size of the zone, the remote applied stress for fault propagation is shown to be less than 100 MPa.

INTRODUCTION

FRACTURE mechanics theory is now an important approach to several areas of earth sciences: analysis of stress distributions around microcracks and faults (e.g. Nemat Nasser & Hori 1982, Hori & Nemat Nasser 1985), the experimental study of sub-critical propagation (e.g. Atkinson 1979, 1980, 1982, Atkinson & Meredith 1981, Cox & Atkinson 1983) and earthquake faulting models and prediction (e.g. Rudnicki 1980, Das & Scholz 1981). The usefulness of the theory in all these areas lies in the simple description of stress and strain around fractures in terms of stress intensity factor (or strain energy release rate, crack extension force or fracture toughness) which can be used to define material constants in a way amenable to experimental determination. The stress around a crack can be given by an expression of the form

$$\sigma = K(2\pi)^{0.5} f(\theta) \qquad (1)$$

in the co-ordinates of Fig. 1 (Lawn & Wilshaw 1975) with K, the stress intensity factor, relating the magnitude of the applied stress field (denoted by subscript L) to the local stress field, in a manner depending on the boundary conditions which can be summarized as

$$K = A\sigma_L(\pi c)^{0.5} \qquad (2)$$

where A is a constant and c the crack half length. Equation (1), based on linear elasticity, therefore predicts infinite stress at the crack tip and draws attention to the fact that the assumption of linear elasticity must break down in a finite region around the crack tip, known as the *process zone* in experimental work (Lawn & Wilshaw 1975).

Microstructural evidence for plastic deformation associated with fracture has been reported in the

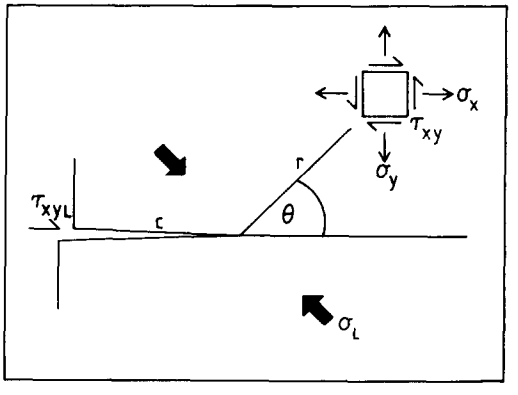

Fig. 1. Co-ordinates used for fracture mechanics analysis of the stress around a mode II crack (after Lawn & Wilshaw 1975).

*Present address: Institute for Crustal Studies, University of California, Santa Barbara, CA 93106, U.S.A.

†Present address: Mineralogy Research Centre, Research School of Chemistry, Australian National University, Canberra, ACT 2601, Australia.

materials science literature (e.g. in zinc, Burns 1970, and lithium fluoride, Burns & Webb 1970). In geological materials, Swanson (1981) detected acoustic emissions from an area ahead of an advancing crack during double torsion experiments on Westerly granite; he suggested that these are manifestations of inelastic behaviour in a process zone that is large compared to the crack length. Peck (1983) observed a greater microcrack density and permeability ahead of the main crack in wedge loading experiments on Sioux quartzite and used this as evidence for a process zone. The process zones in Charcoal and Rockville granites are described in detail by Labuz *et al.* (1987) using ultrasonic probing and acoustic emission to characterize the size of these regions of inelastic behaviour at the crack tip. Theoretical values for the size of the process zone in crustal faulting have been calculated by Rudnicki (1980). However, no examples of process zones from naturally deformed rocks have so far been reported.

The aim of this study is to present evidence for a process zone from samples on a fault in quartzite from the northwest of Spain, and to elucidate the faulting mechanisms. The microstructures are described, and a fracture mechanics analysis is used to model the crack propagation and deduce the stress system that operated during faulting. The stress estimates were obtained from quartz microstructural palaeopiezometers including deformation lamellae (Koch & Christie 1981, Drury & Humphreys 1987) and dislocation densities (Twiss 1986). This study emphasizes the problem of interpreting stress measurements from palaeopiezometers, in which crack tip or process zone stresses must be distinguished from remote applied stresses.

FIELD RELATIONS

The samples described are from the Bayas Fault on the headland of Punta Vidrias in the north part of the Somiedo–Corecilla nappe unit of the Cantabrian zone (CZ). The CZ is the most external zone of the Ibero–Armorican Arc, the structural feature that represents the Variscan Orogen in northwest Spain and Brittany (Figs. 2 and 3). It is a foreland fold-and-thrust belt, showing many typical features of thin-skinned thrust tectonics in a sequence of variable, Lower Palaeozoic shallow marine shelf sediments. These include the thick, pure, white quartzite (Barrios Formation) from which all the samples in this study are taken. The overall structural style and the development of the external part of the arc have been discussed by Julivert (1971), Julivert & Marcos (1973), Julivert & Arboleya (1984, 1986) and

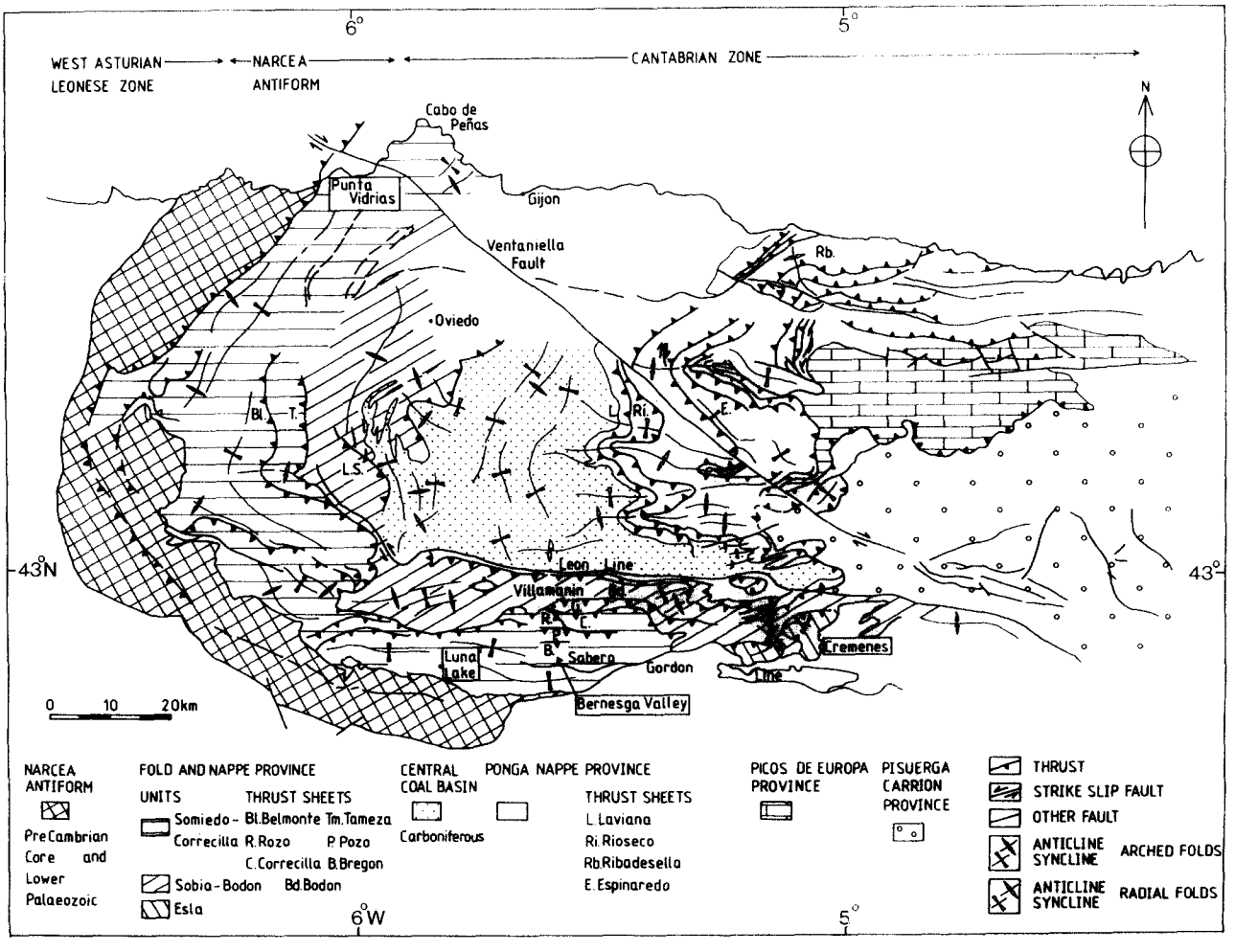

Fig. 2 Structural units of the Cantabrian zone, N.W. Spain (after Julivert 1971).

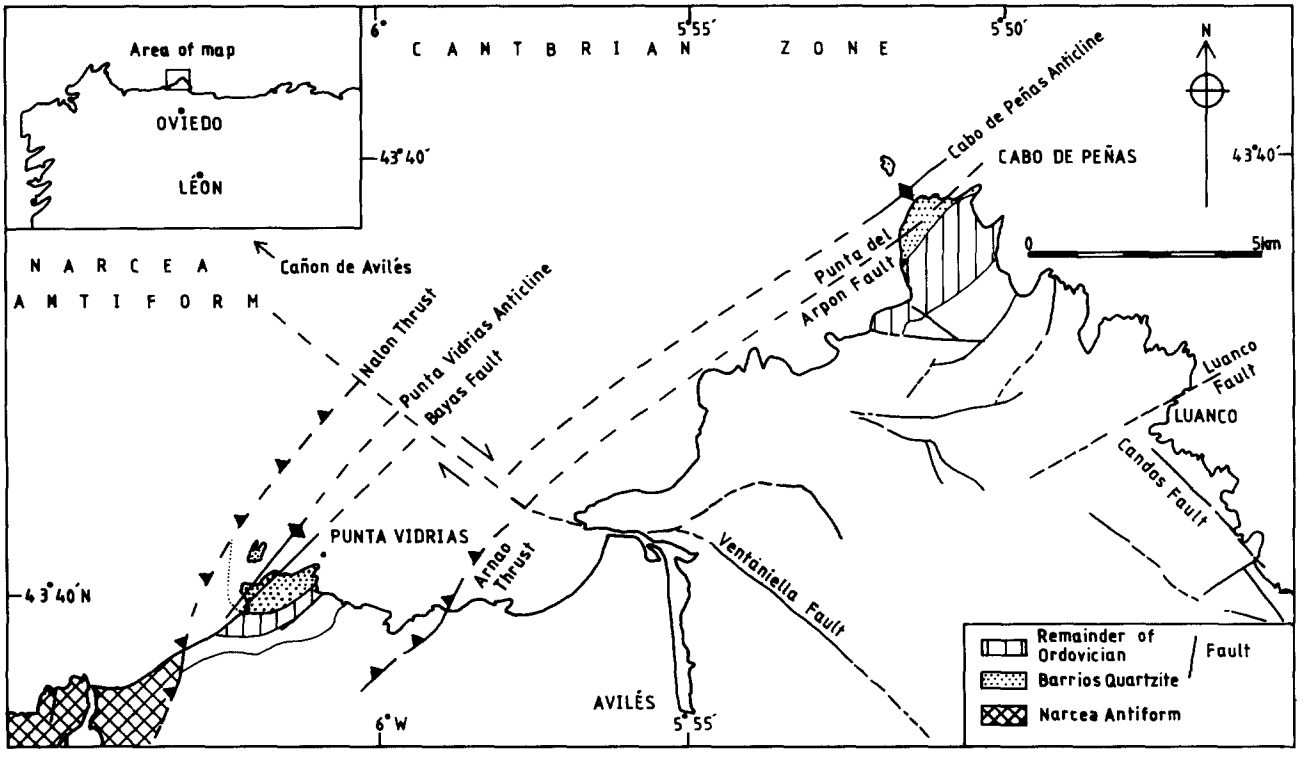

Fig. 3 Major structures and locations of Punta Vidrias and Cabo de Peñas (data from I.G.M.E. Mapa Geologico de España, 1:50,000 Aviles).

most recently by Pérez-Estaún *et al.* (in preparation). In the latter, evidence is summarized for the primary (pretectonic) curved shape of the arc, its subsequent tightening during orogeny (based on the palaeomagnetic work of Ries *et al.* 1980, Perroud & Bonhommet 1981, Perroud *et al.* 1984), and the clockwise sequential movement of nappe units, beginning in the southwest with the Esla Nappe (Fig. 2) and finishing with the S-directed movement of the Picos de Europa.

The timing of deformation can be fairly well constrained for some parts of the C.Z. Course alluvial fan deposits in the south of the Sobia–Gordon unit have been related to the movement of the Somiedo–Correcilla unit by Marcos & Pulgar (1982) indicating that a foredeep trough migrated ahead of the thrust front during Westphalian B–D. However, an earlier start for the onset of deformation has been inferred by Blenkinsop (1987) from the presence of widespread unconformities throughout the southern part of the C.Z. during Fammenian times. This may also apply to the northern part of the C.Z. The main deformation was probably complete by the uppermost Westphalian.

Some inferences about the conditions of deformation can be made from the rapidly accumulating clay mineralogy and illite crystallinity data for the C.Z. In most of the C.Z. the temperature never exceeded that of the diagenetic zone (Brime 1985, Blenkinsop 1987). However, there are increases in illite crystallinity up to the anchizone at the base of the thrust sheets in the Somiedo–Corecilla nappe unit, and in the north of the zone. The former pattern has been interpreted as a preserved burial diagenetic gradient by Blenkinsop, while the latter may reflect a local source of heat which intensifies towards Cabo de Peñas (Fig. 3). A temperature range of 148–248°C has been deduced for the Punta Vidrias area from shale crystallinities. The maximum stratigraphic depth of burial can be estimated as 4.0 km at Punta Vidrias, although there was probably a further component of tectonic overburden. Therefore the minimum confining pressure was 100 MPa using a lithostatic stress gradient of 25 MPa km^{-1}. Pore fluid pressures are assumed to be hydrostatic in the quartzites during deformation since it can be established that there was a pervasive fracture network operating during the deformation (see below). Effective confining pressure was therefore 60 MPa, assuming a ratio of pore fluid pressure to lithostatic stress (λ) of 0.4.

The Barrios Formation is a fine- to medium-grained quartzite (grain size 100–200 μm) with a variable amount of quartz cement. Porosities are estimated to have been from 4 to 13% before deformation and minor components of iron oxides, detrital phyllosilicates and clay minerals may form up to 16% of the rock.

In the study area, the Barrios Formation is folded into a large, SE-verging, gently inclined anticline, which plunges at 20°/218°. This is shown in Fig. 3 as the Punta Vidrias Anticline. A similar structure is visible at Cabo de Peñas and it is evident by extrapolation of the axial traces along strike that they meet at the offshore position of the Ventaniella Fault, where they are displaced dextally by 3 km (Fig. 3). This is also the sense and amount of displacement that can be shown for the Ventaniella Fault onshore to the southeast from Hercynian features (e.g. thrusts, folds and deformed bedding). The two

folds are undoubtedly equivalent. Using evidence of folded cleavage, Julivert (1976) has shown that this structure is but the upper part of an earlier isoclinal fold, later refolded homoaxially; indeed open crescent forms, indicating fold interference structures, can be seen in the outcrop of the lower Palaeozoic further inland. The Nalon Thrust is exposed at the coast 3 km southwest of Punta Vidrias, where it places the Precambrian Hererria formation over Silurian–Devonian sediments (Fig. 3).

A general feature of the Barrios Formation in the study area is the presence of a ubiquitous fracture network. These fractures occur in three or more sets, always subperpendicular to bedding, so that their poles form a girdle around the pole to bedding. This bedding-perpendicular 'necklace' of fractures is rotated with the bedding around the fold axis, and may be the main deformational mechanism that accommodated folding (Blenkinsop 1987). They evidently formed before the fold and allowed necessary fold strains by small movements along the pre-existing fractures.

MACRO- AND MESO-SCALE FEATURES OF THE BAYAS FAULT

The Bayas fault plane is exposed on the Playa de Bayas where it forms a low vertical scarp that dies out inland (Fig. 4a & b). Fault planes with similar orientations can also be seen at Punta del Moro, Punta del Arpon and at the kaolinite mines on the headland at Cabo de Peñas (Fig. 3). The fault surface at Playa de Bayas is corrugated on two scales: larger *undulations* with sinusoidal profiles and cylindrical axes have wavelengths of 2 m and amplitudes of 100–200 mm (Fig. 4a); much smaller slickenside lineations have irregular terminations, wavelengths of tens of mm and amplitudes of 1 mm. Both corrugations plunge northeast at 30° and bedding shows a horizontal dextral displacement of 100 m. The fault has a dull grey polished surface, and is cut by a set of large fractures normal to the plane with dominantly mode I displacements of 50 mm (Fig. 4b). Most of these are filled by quartz breccia, rosettes of barytes needles 20–30 mm long, and distinctive, very fine-grained, black quartz, which is also observed to penetrate the fault surface in thin anastomosing veins. The dilatant fractures normal to the fault plane cut a set of smaller quartz veins that are subparallel to the fault. These features are summarized in Fig. 6 and their orientations in the stereogram of Fig. 7.

MICROSTRUCTURES OF THE BAYAS FAULT

Thin sections show that the fault zone consists of a layer of cataclasite several tens of mm thick extending southeast from the vertical fault surface. The northwest side of the fault is not exposed. Clusters of several tens of grains of wallrock are surrounded by a matrix of fine-grained quartz within the cataclasite, in which three components can be identified by cathodoluminescence (C.L.) (Fig. 4c): luminescing angular fragments of grains, non-luminescing matrix and fine-grained iron oxides. The cataclasite layer is separated from unsheared wall rock by stylolites. All features are cut by the larger dilatant veins normal to the fault and the network of small anastomosing dark veins.

Vein material

The black quartz is seen in optical thin section to owe its color to a high density of extremely fine-grained iron oxide particles. The use of C.L. in conjunction with an image and microanalysis system enables subtle contrasts in luminescence to be effectively discriminated. In Fig. 4(c), the dark vein consists of the black quartz that permeates the fault surface: it is differentiated from the cataclasite matrix by the lack of grain fragments. Intragranular crack fills within grain fragments are also dark. In the same field of view but separated by a different amplitude of luminescence, Fig. 4(d) shows both vein material and ultracataclasite as bright areas, and grain fragments with their intragranular crack cements are dark. The final view of the same area (Fig. 4e) highlights intragranular cements and iron oxide particles. These three views establish that grain fragments, intragranular crack cements, cataclasite matrix and black veins each have a unique luminescence, implying separate sources.

The larger dilatant veins are spectacular features in C.L. Figure 5(a) shows very brilliant luminescence from patches of iron oxides, bright luminescence from barytes and an area of mottled texture. Under high magnification, it is seen that the mottled texture is a fine-grained intergrowth of iron oxides, barytes and quartz (Fig. 4f).

Wall rock

Both the unsheared wall rock and the clusters of grains in the cataclasite are notable for three features that are restricted to samples within 3 m of the fault; they are not observed anywhere else on the Punta Vidrias headland.

(1) *Microfractures.* C.L. shows both intra- and transgranular microfractures (e.g. Fig. 4c), which are also seen using light microscopy as lines of bubbles (Fig. 5b). They have a strong preferred orientation within individual clusters, but are rotated between adjacent clusters. We have also imaged a feature in T.E.M. that we believe is a sealed microcrack. Figure 5(c) shows that it has straight walls, a low density of straight dislocations and a high density of radiation damage centres in bands parallel to the walls. The former feature has been described for pressure-shadow fringes of quartz (White 1973), and the latter for quartz cements in cataclasites (Stel 1981), suggesting that the features observed are cemented microcracks.

(2) *Deformation bands.* There are between one and 10 deformation bands in almost every unsheared grain (Fig. 5b), which are sub-parallel across entire clusters of grain fragments, usually perpendicular to the microfractures. Like the microfractures, the orientation of the

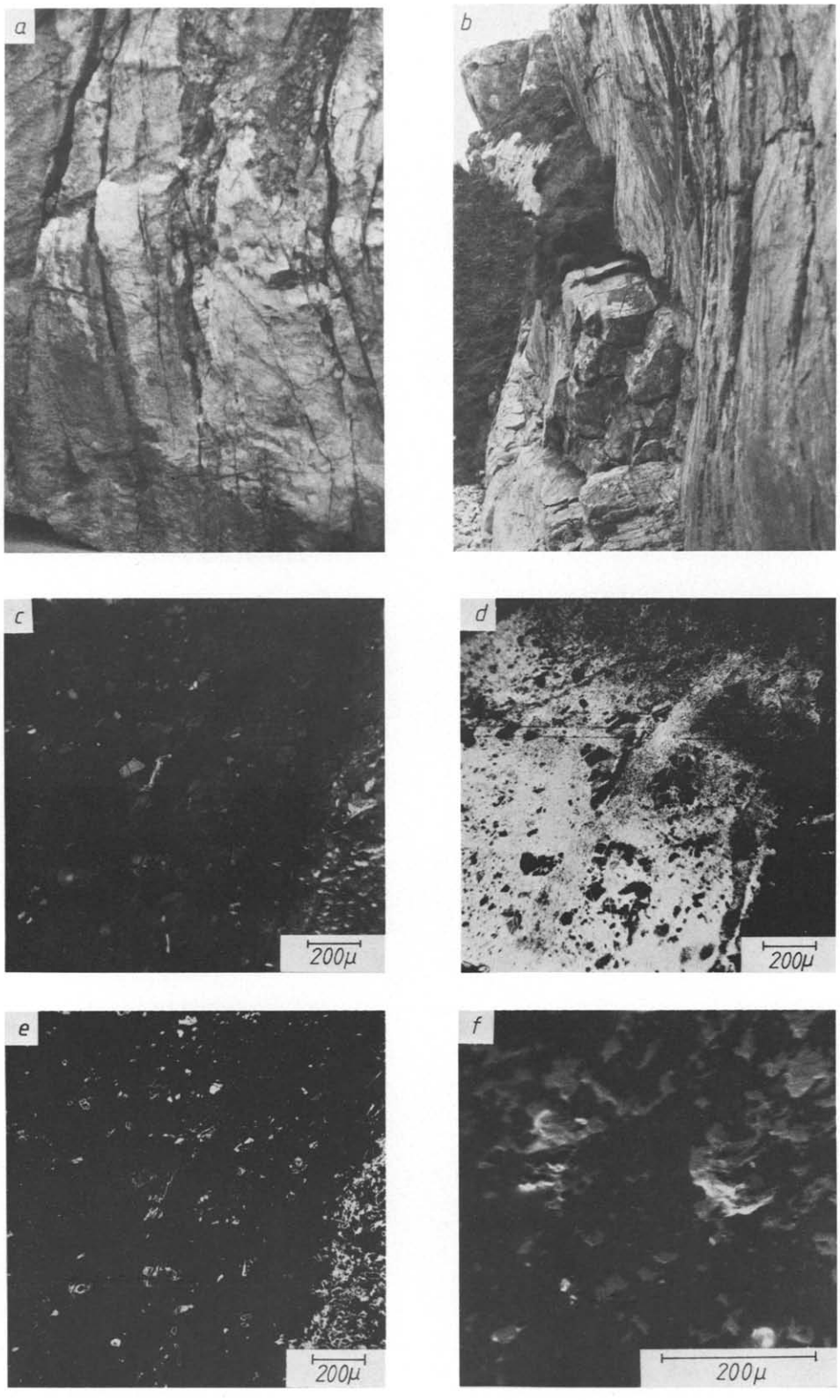

Fig. 4. (a) Bayas fault plane, showing undulations, lineations and large dilatant fractures either open or filled with black quartz, quartz breccia and barytes. Height of view approximately 2 m; NE to left. (b) Profile view of the Bayas fault plane. The undulations are clearly visible, and displacements are seen on bedding planes and large fractures perpendicular to the fault plane. Height of scarp approximately 20 m. View towards NE. (c) Cataclasite matrix of the Bayas fault zone in cathodoluminescence (C.L.). (d) Grain fragments luminesce in the dark cataclasite matrix. The black vein has very few grain fragments, and hence is distinguished from the cataclasite matrix. Intragranular cracks within the grain fragments are also dark. (e) In the same view, intragranular cements and iron oxides only are bright. (C.L.) (f) Detailed view of mottled texture in cathodoluminescence. The texture is a fine-grained intergrowth of iron oxides, barytes and non-luminescing quartz cement.

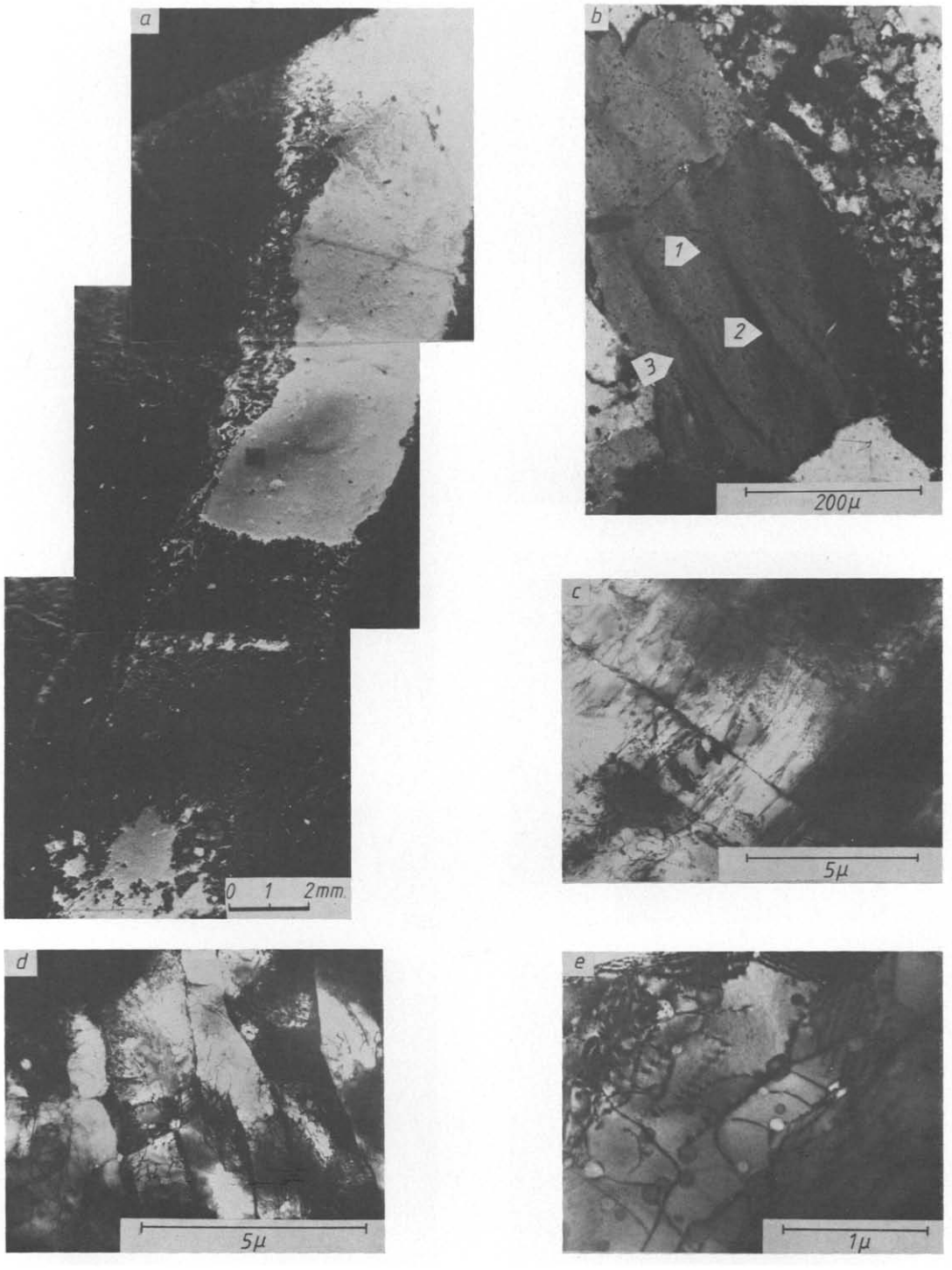

Fig. 5. (a) Large dilatant vein in cathodoluminescence. The most brilliant luminescence is from patches of iron oxides. Barytes in large areas is also brightly luminescing, and the mottled texture is also seen. (C.L.) (b) Optical photomicrograph of a cluster of wall rock grains in cataclasite from the Bayas fault plane. Three features can be identified. (1) Microfractures. Curved lines of bubbles or inclusions. (2) Deformation bands. Triangular shaped bands of extinction contrasts with poorly defined edges. (3) Deformation lamellae. Sharply defined, extremely narrow bands perpendicular to deformation bands (crossed-polars). (c) T.E.M. view of microfractures. A low density of straight dislocations, and high density of radiation damage centres in bands parallel to the sharp edges of the lamellae are diagnostic of precipitated quartz. (d) T.E.M. view of banded substructure which defines the deformation lamellae. The boundaries of the structure consist of curved dislocation walls made up of dense well-ordered arrays of two or three sets of dislocations. (e) Average dislocation density and high density of fluid inclusions from the deformation lamellae. Note occurrence of very low angle dislocation walls and networks inside the banded substructure, and the interlinking of dislocations forming a coarse network with fluid inclusions at the nodes.

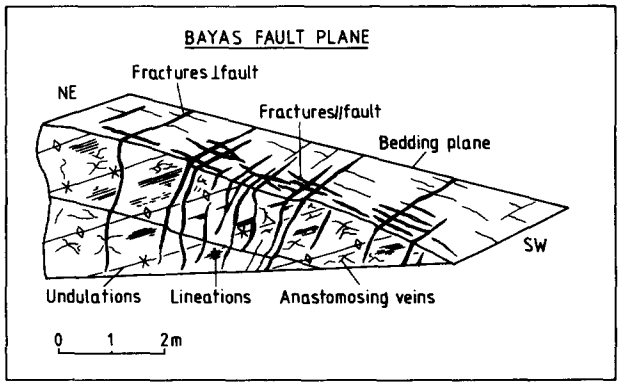

Fig. 6. Fault plane features of the Bayas Fault.

deformation bands is rotated between adjacent grain clusters. They have diffuse and curved walls forming needle shaped sections up to 10 μm wide.

(3) *Deformation lamellae.* Fine-scale deformation lamellae appear as thin lines a few μm thick and tens of μm long using optical microscopy (Fig. 5b). These form perpendicular to the deformation bands. In T.E.M., they consist of elongate subgrains 1.5 μm wide, with a sub-basal orientation (cf. Ave Lallement & Carter 1971), bounded by curved dislocation walls made up of well ordered arrays of two to three sets of dislocations (Fig. 5d). They may have high fluid inclusion densities and variable dislocation densities from 4×10^{12} to 2×10^{13} m^{-2} (measured over a total area of 80 μm^2 at 11 sample sites in four grains). The dislocations interlink to form a coarse network with inclusions at the nodes (Fig. 5e). This arrangement suggests that the internal structure of the deformation lamellae subgrains is highly recovered.

EVOLUTION OF THE BAYAS FAULT

Figure 3 shows that the Bayas Fault may link with the fault of similar orientation at Punta del Arpon, in which case it is displaced by the post-orogenic movements on the Ventaniella Fault. The fault does not appear to be folded by the Punta Vidrias Anticline and the dilatant fractures associated with the fault plane clearly cross-cut bedding normal fractures of the sets that formed before the large fold. The fault was therefore formed after the folding but before the major dextral movements on the Ventaniella Fault, which Marcos (1979) has suggested may be Permian. There is a regionally developed set of dextral strike-slip faults to the east of the area, with strikes from 107 to 125°, some of which displace regional thrusts. These have been interpreted by Pérez-Estaún (personal communication) as late fractures reflecting the closure of the Ibero-Armorican Arc, as required by the palaeomagnetic data. The dextral displacement on the Bayas Fault is compatible with this kinematic picture, and the timing (post-folding and thrusting, pre-Permian) suggests that the Bayas Fault is coeval with the regional dextral strike-slip fault set.

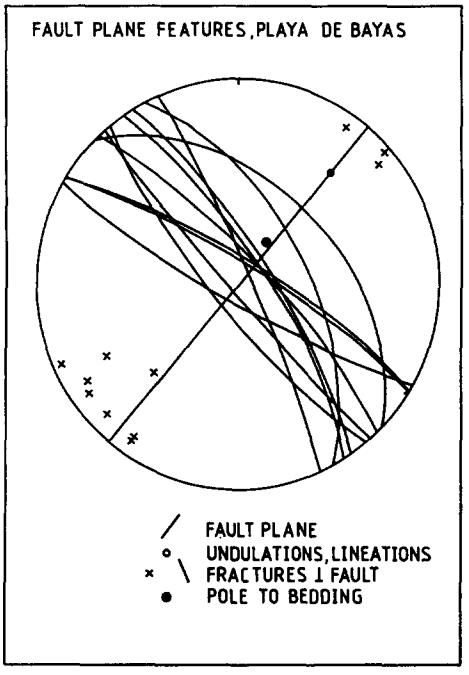

Fig. 7. Orientation of the Bayas fault plane features. Equal-area, lower-hemisphere projection.

The two scales of corrugation of the fault surface may have formed in different ways, although both are parallel to the inferred displacement direction of the fault. The large undulations do not have stepped terminations that might be interpreted as products of differential movement between the sides of the fault. Rather, they probably represent the original morphology of the fault surface. A non-linear profile in the plane normal to the displacement direction has been reported for faults in the Entrada sandstone by Aydin & Johnson (1983) and can be deduced for much smaller microfaults in the Westphalian conglomerate that outcrops in the Central Coal Basin (Fig. 1) where corrugations of the fault surface are clearly much longer than the negligible shear displacements on the microcracks. However, the slickenside lineations do have irregular ends suggesting that they may be conventional wear grooves.

The earliest deformation mechanism in the fault zone was crystal plasticity, in the form of deformation lamellae and deformation bands, confined to a zone less than 3 m from the fault. It has been shown for metals that lamellae develop after strains of 5–10%; thereafter, at higher strains (>20%), deformation bands form (Drury & Humphreys 1986). There is evidence for repeated cycles of cataclasis and cementation: the variable luminescence of microcrack cement, vein material and ultracataclasite matrix suggests multiple generations of quartz cements. The cataclasite formed by detachment of clusters of unsheared grains from the fault walls and their attrition by microcracking. This clearly post-dates the plasticity since crack cements have low dislocation densities. The large dilatant veins were opened and filled by breccias from the fault surface and barytes and quartz cements. The latest event was the development of stylolites between the cataclasite and the wall rock: they may therefore be unrelated to the faulting.

The association of dilatancy and multiple faulting episodes was the observational basis leading to the proposal of the seismic pumping mechanism by Sibson *et al.* (1975). We likewise suggest that the vein features observed here may be the products of a seismic pumping mechanism. We can further distinguish between the possibility that the fluid pressure drove the faulting and the reverse situation, in which the faulting, in response to the applied stress, drove the fluids. Since the dilatant veins commonly contain considerable quantities of quartz breccia that must be derived from the fault plane (there is no appreciable shear displacement on the dilatant veins), it is more likely that the breccia was generated on the fault plane and subsequently injected into the veins as the fault moved—the fluids and breccia being mobilized by faulting. Furthermore, pore fluid pressures were unlikely to be higher than hydrostatic because of the pre-existing fracture network in the quartzites.

STRESS ESTIMATES FROM THE BAYAS FAULT PLANE

The occurrence of deformation lamellae can be used to provide a stress estimate for the Bayas Fault zone. The recovered slip band structure of the quartz lamellae is similar to structures observed in deformed metals. In metals and ionic minerals there is strong evidence that deformation lamellae are a characteristic microstructure of the power-law-breakdown (PLB) creep regime (Heard 1972, Drury & Humphreys 1986). In this regime an exponential relationship holds between steady state strain rate and stress (Frost & Ashby 1982, Tsenn & Carter 1987). PLB creep is thought to represent a transition regime where both recovery-controlled and glide-controlled deformation mechanisms are operative (Nix & Ilscher 1979, Frost & Ashby 1982, Tsenn & Carter 1987). It is likely that deformation lamellae represent the microstructural expression of the localized glide component of the deformation (Drury & Humphreys 1987).

Experiments on a wide range of materials have shown that PLB creep occurs above a critical stress that is a characteristic of classes of materials when normalized by their shear modulus (Sherby & Burke 1968, Tsenn & Carter 1987). The values of the critical normalized stress for PLB increases with increasing crystal bond strength of the material (Drury & Humphreys 1987, Tsenn & Carter 1987). Unfortunately the data for quartz are poorly constrained and inconsistent (Drury & Humphreys 1987). Some studies suggest a transition stress to a PLB regime at about 400 MPa (Heard & Carter 1968) while others indicate higher values of up to 1000–2000 MPa (Koch *et al.* 1980, Jaoul *et al.* 1984). While the rheological data are inconsistent there is experimental microstructural evidence for a critical stress for the development of extensive sub-basal lamellae of about 200–400 MPa (Tullis *et al.* 1973, Jaoul *et al.* 1984). In the absence of a suitable calibration for quartz a lower estimate for the normalized critical shear stress of 3×10^{-3}–4×10^{-3} can be obtained from the reliable data on ionic minerals (Schmidt *et al.* 1977, 1980, Spiers *et al.* 1986, Tsenn & Carter 1987), as the critical stress for lamellae increases with increasing crystal bond strength. An upper estimate of 420 MPa can be obtained from the upper experimental value (Drury & Humphreys 1987). These estimates indicate that sub-basal deformation lamellae can be used as indicators of deviatoric stresses of at least 170 MPa. In the following analysis of fault propagation, 170 and 420 MPa will be used as representative lower and upper estimates of the critical stress for the development of lamellae.

The optically measured spacing of deformation lamellae can also be used as a palaeopiezometer using the calibration of Koch & Christie (1981) on experimentally deformed natural quartzites. A differential stress of 180 MPa is obtained using this method for the lamellae in Fig. 5(b).

Dislocation densities have been used as a second palaeopiezometer following the experimental calibration of McCormick (1977). This yields a value of 116 MPa. An important limitation on the reliability of this estimate is the fact that the calibration was obtained on synthetic quartz. The mechanical behaviour of synthetic quartz is significantly different from that of most natural quartz (e.g. Paterson & Kekulawalla 1979). Experimental results on natural quartzites (Koch 1983) are, however, consistent with the calibration of McCormick (Twiss 1986). The coarse dislocation network observed in the present work suggests a highly recovered structure within the deformation lamellae. Thus stress estimates using dislocation densities must be regarded as a minimum as recovery subsequent to deformation reduces the dislocation density. Twiss (1986) has also pointed out that there are problems with extrapolation of experimental data to lower natural stresses. This drawback does not apply in this study, where dislocation densities are in the same range as in the experiments of McCormick (1977).

Better calibration of the deformation lamellae palaeopiezometer must await a comprehensive experimental program. In the meantime, the rather poor constraints on the data are allowed for by considering the range of values between 170 and 420 MPa.

DISCUSSION: THE CRACK TIP PROCESS ZONE MODEL

The microstructures described above indicate a deformation history consisting of an early period of crystal plasticity at high stress confined to the fault zone, followed by episodic displacement and cementation. The early and restricted nature of the plasticity points towards the existence of a process zone that operated in front of the crack tip. In the following, a model is proposed in which the deformation lamellae and bands are generated in this process zone, and the cataclastic features by subsequent movement of the main fault

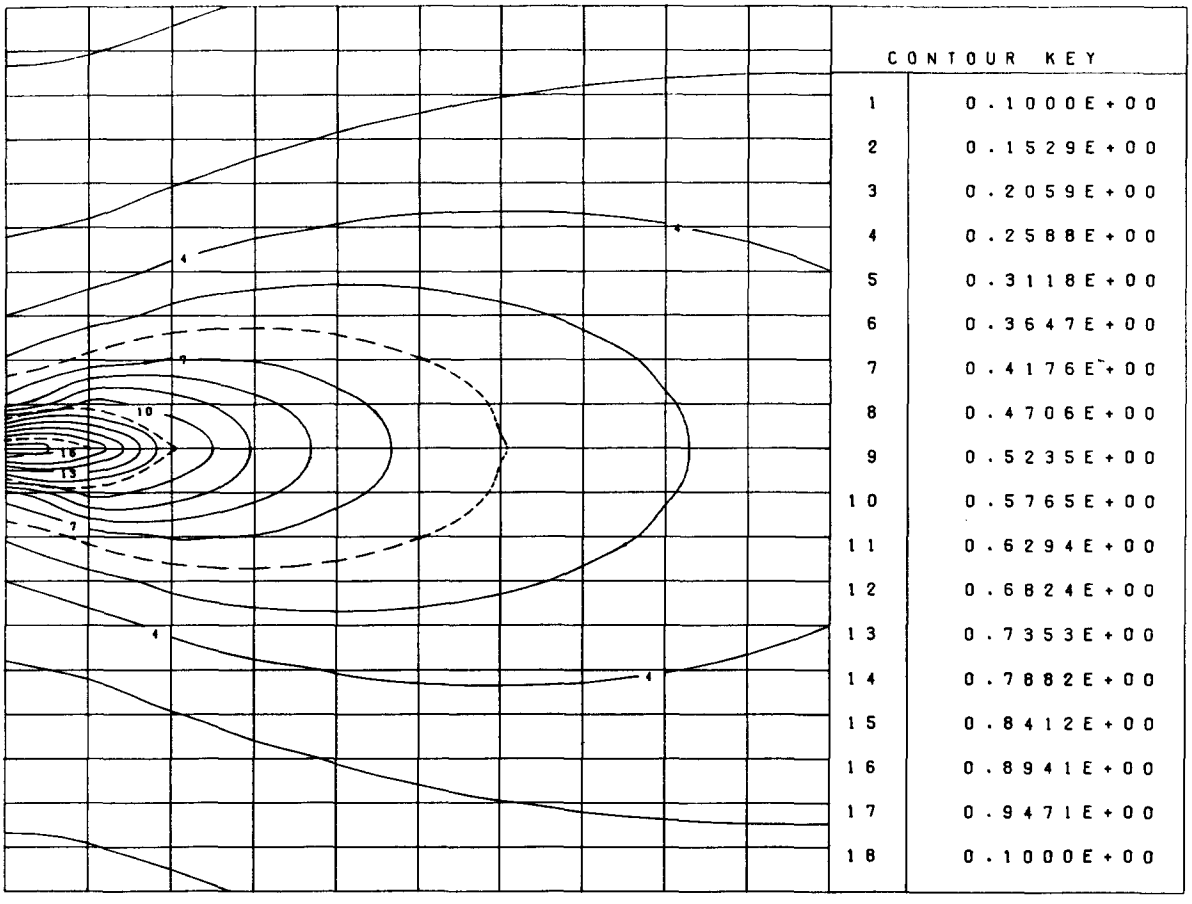

Fig. 8. Contours of differential stress around a mode II crack tip calculated from equation (3). The values of the contours are in units of 100 MPa for remote differential stress ($\Delta\sigma_L$) of 100 MPa applied to a crack half length (c) of 10 m. The grid lines are at intervals of 1 m. The crack tip is at 0; the crack (not shown) extends to the left.

plane. The available constraints are used to show that the model is realistic.

The fault is treated as a pure mode II crack, for which the stresses in the co-ordinates of Fig. 1 (after Lawn & Wilshaw 1975) are

$$\sigma_x = K_{II} f_x(\phi)/2\pi r^{0.5}$$
$$\sigma_y = K_{II} f_y(\phi)/2\pi r^{0.5}$$
$$\tau_{xy} = K_{II} f_{xy}(\phi)/2\pi r^{0.5},$$

where K_{II} is the critical stress intensity factor for mode II crack propagation, given by $\tau_{xyL}(\pi c)^{0.5}$ with τ_{xyL} the remote applied shear stress and c the crack half length. The functions $f(\phi)$ are

$$f_x(\phi) = -\sin(\phi/2)\{(2 + \cos(\phi/2)\cos(3\phi/2)\}$$
$$f_y(\phi) = \sin(\phi/2)\cos(3\phi/2)$$
$$f_{xy}(\phi) = \cos(\phi/2)\{(1 - \sin(\phi/2)\sin(3\phi/2)\}.$$

Substituting for these, using the expression for K_{II} (equation 2), and transforming to principal stresses, the following expression can be derived for differential stress ($\sigma_1 - \sigma_3 = \Delta\sigma$) in front of the crack tip

$$\sigma_1 - \sigma_3 = \tau_{xyL} c^{0.5}(f_{xy}(\phi)^2 + 0.25(f_x(\phi) - f_y(\phi)^2)^{0.5}/\pi^{0.5} r^{0.5}. \quad (3)$$

Contours of $\Delta\sigma$ around the crack tip are shown in Fig. 8 and a surface view of these values in Fig. 9 (an arbitrary maximum value has been given to the stress at the crack tip itself). Profiles of the differential stress in the direction of crack propagation and perpendicular to it are shown in Fig. 10 for crack half lengths of 0.1, 1 and 10 m with an applied stress of 100 MPa. It is proposed that the infinite increase in stress towards the crack tip is relieved by crystal plasticity in the crack tip process zone. We can therefore use the stress estimates for the formation of deformation lamellae and Fig. 10 to calculate the size of the process zone in front and to the side of the crack. This is shown diagrammatically in Fig. 11. The size of the process zone for remote applied stresses of 10, 100 and 250 MPa as a function of crack half length and for both estimates of critical stress for the formation of lamellae

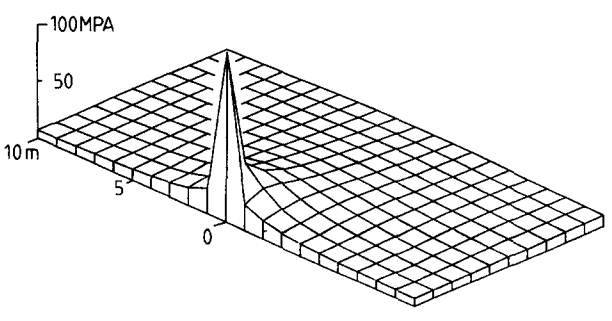

Fig. 9. Surface view of differential stress in front of a mode II crack tip, for the same conditions as Fig. 8. The stress at the crack tip itself has been set to an arbitrary maximum to allow completion of the drawing.

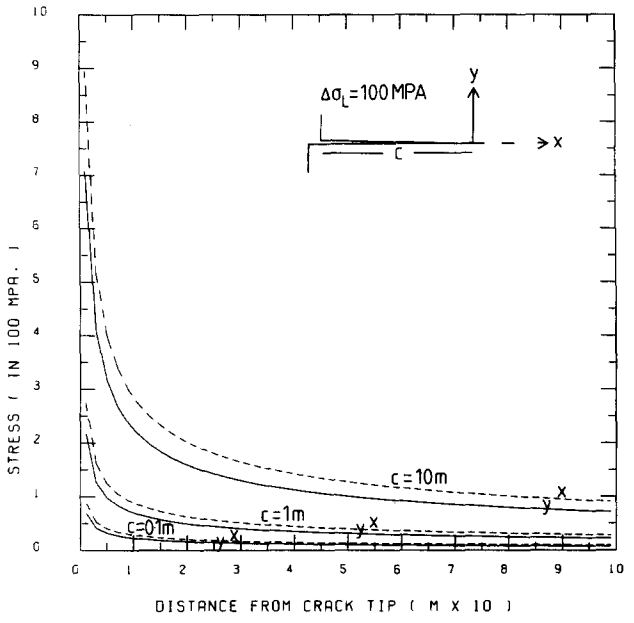

Fig. 10. Differential stress as a function of distance from the crack tip. Each pair of lines shows the relationship in the direction of crack advance and perpendicular to the crack (dashed, x, and full, y, respectively) for crack half lengths (c) of 10, 1 and 0.1 m and a remote applied differential stress ($\Delta\sigma_L$) of 100 MPa.

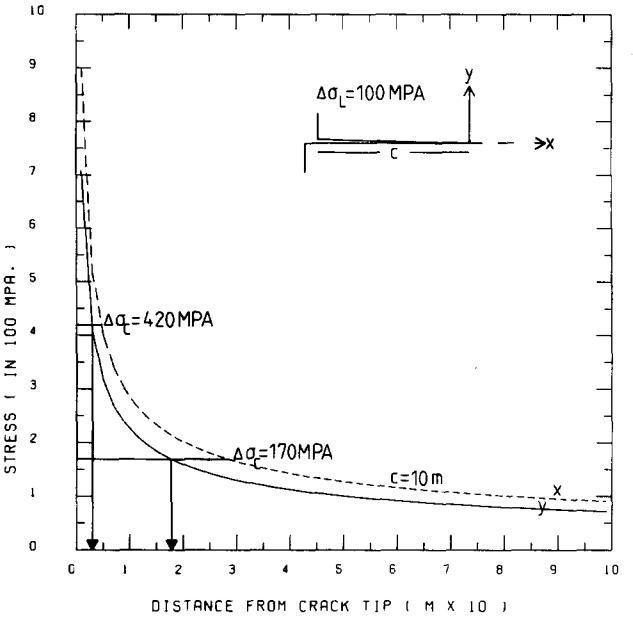

Fig. 11. Diagram to show how the size of the process zone can be established from the value of stress estimated from the presence of deformation lamellae (170 and 420 MPa), and the decrease of stress away from the crack tip (as in Fig. 10).

are shown in Fig. 12. Differential stresses of 170 MPa and greater are established within 2 m of the crack tip for the entire range of likely remote applied stresses. The estimates of the size of the process zone for remote applies stresses of 100 MPa have the same range (1–100 mm) for crack lengths of 0–10 m as deduced for crustal process zones by Rudnicki (1980).

A maximum value for the actual size of the process zone of the Bayas Fault can be deduced from the fact that no deformation lamellae are observed at a distance of 3 m perpendicular to the fault zone. It is possible to calculate the remote applied stress as a function of crack half length and critical stress for the formation of lamellae given the known size of the process zone. This is shown in Fig. 13 together with the stresses calculated for the smaller process zones of 1 and 0.1 m. The remote applied stress falls to less than 100 MPa for the more likely value of 0.1 m (see above) by the time the crack has reached a length of 6 or 37 m for process zone stresses of 170 and 420 MPa, respectively.

The importance of the pre-existing fracture network to the success of the model is now clear. Fractures of an appropriate length were available before folding of the Punta Vidrias Anticline, so that the Bayas Fault could have been initiated at stresses of 100 MPa or less. The fault may have followed one of the fracture sets, favourably orientated in the core of the anticline, and propagated by linking up fractures of this set so that its effective length never exceeded a few tens of metres, the maximum spacing between fractures. In this model, mode II fault propagation occurred when the fault linked pre-existing fractures. This fracture mode is difficult to demonstrate in geological materials although it has been shown from calcite twins adjacent to thrust planes by both Hyett (presented at Tectonic Studies Group Annual General Meeting, 1985) and Rutter & Rowe (presented at Palaeostress and Fault Systems Meeting, University of Swansea, 1987). The stress orientations deduced from the twins agree well with the theoretical orientations expected around a mode II crack. Although the model has not been tested in great detail, its importance can be established both as a conceptual approach and as a realistic description of the fault propagation.

Shear zone propagation has also been modelled by mode II crack stress fields by Norton (1982) and Attfield & Kusznir (presented at Tectonic Studies Group Annual General Meeting, 1985). The very high stresses com-

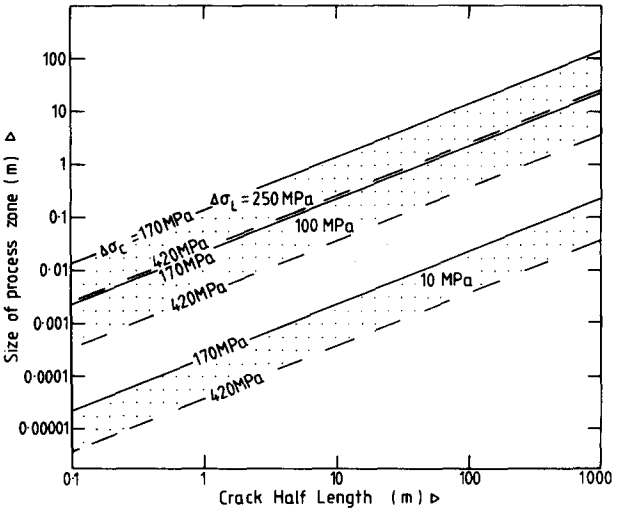

Fig. 12. Size of the process zone perpendicular to the crack as a function of crack half length. Each pair of lines shows the relationship assuming process zone stress ($\Delta\sigma_c$) of 170 and 420 MPa (solid and dashed lines, respectively), delineating the stippled bands for remote applied stress ($\Delta\sigma_L$) of 250, 100 and 10 MPa. The process zone sizes are in the same range as those estimated by Rudnicki (1980), for a remote stress of 100 MPa applied to crack half lengths of 0–10 m.

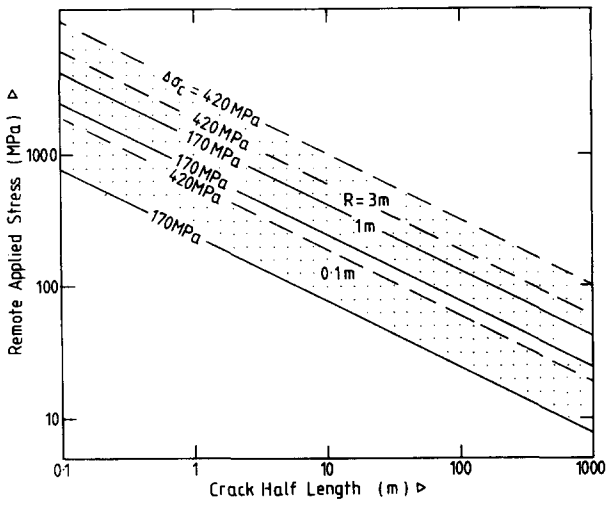

Fig. 13. Remote applied stress as a function of crack half length. Each pair of lines shows the relationship assuming process zone stresses ($\Delta\sigma_c$) of 170 and 420 MPa (solid and dashed lines, respectively), delineating the stippled bands for process zone size R, perpendicular to the crack, of 3, 1 and 0.1 m. For the most likely value (0.1 m), the remote applied stress is less than 100 MPa at crack half lengths of 6 or 37 m. Cracks of this size existed before faulting.

monly measured by palaeopiezometers in the central parts of shear zones may be caused by crack tip stress concentration. Experimental studies on the development of mylonitic shear zones in rock analogues (Drury *et al.* 1982, White *et al.* 1985) have shown that the recrystallized grain sizes developed during high stress initiation are preserved during high strain deformation at lower stress. It is important to differentiate crack tip stresses from applied crustal stresses.

CONCLUSIONS

(1) The Bayas Fault propagated by an initial crystal plastic mechanism (power-law-breakdown creep) localized in a process zone ahead of the fault plane, followed by episodic cataclasis with extensive veining and dilatancy. A seismic pumping mechanism, driven by variations in the applied stress, is envisaged.

(2) Deformation bands and lamellae were formed during the crystal plasticity. The deformation lamellae can be used to provide a minimum stress estimate of 170 MPa, which is supported by a minimum value of 116 MPa given by partly recovered dislocation densities, and a value of 180 MPa from the spacing of lamellae (Koch & Christie 1981).

(3) The deformation lamellae formed in a process zone ahead of the advancing fault. The stress system is realistically modelled by a mode II crack, which was probably initiated on a pre-existing fracture.

(4) Applied crustal differential stresses of only 100 MPa or less are quite sufficient to drive the faulting. This estimate is consistent with other average crustal stress estimates (e.g. Tsenn & Carter 1987).

Acknowledgements—The co-operation of the staff of Keele University is gratefully acknowledged. We also thank Dr E. H. Rutter and two anonymous referees for improvements made to the manuscript.

REFERENCES

Atkinson, B. K. 1979. A fracture mechanics study of subcritical tensile cracking of quartz in wet environments. *Pure & appl. Geophys.* **117**, 1011–24.

Atkinson, B. K. 1980. Stress corrosion and the rate dependent tensile failure of a fine-grained quartz rock. *Tectonophysics* **65**, 281–290.

Atkinson, B. K. 1982. Subcritical crack propagation in rocks: theory, experimental results and applications. *J. Struct. Geol.* **4**, 41–56.

Atkinson, B. K. & Meredith, P. G. 1981. Stress corrosion cracking of quartz: a note on the influence of chemical environment. *Tectonophysics* **77**, T1–T11.

Ave Lallement, H. G. & Carter, N. L. 1971. Pressure dependence of quartz deformation lamellae orientations. *Am. J. Sci.* **270**, 218–235.

Aydin, A. & Johnson, A. M. 1983. Analysis of faulting in porous sandstones. *J. Struct. Geol.* **5**, 19–31.

Blenkinsop, T. G. 1987. Mechanisms and conditions of deformation in quartzites from the Cantabrian and West Asturian–Leonese zones, N.W. Spain. Unpublished Ph.D. thesis, University of Keele, U.K.

Brime, C. 1985. Diagenesis to metamorphism transition in the Hercynian of north-west Spain. *Mineralog. Mag.* **49**, 481–484.

Burns, S. J. 1970. Dislocation motion accompanying cleavage in zinc. *Acta metall.* **18**, 969–980.

Burns, S. J. & Webb, W. W. 1970. Fracture surface energies and dynamic cleavage of LiF. I—Theory. II—Experiments. *J. appl. Phys.* **41**, 2078–2095.

Cox, S. J. D. & Atkinson, B. K. 1983. Fracture mechanics and acoustic emission of anti-plane shear cracks in rocks. *Earthquake Pred. & Res.* **2**, 1–24.

Das, S. & Scholz, C. H. 1981. Theory of time-dependent rupture in the Earth. *J. geophys. Res.* **86**, 6039–6051.

Drury, M. R., White, S. H. & Humphreys, F. J. 1982. The development of a shear band foliation in a rock analogue. *Mitt. Geol. Inst. E.T.H. Univ. Zurich. Neue Folge* **239a**, 84–87.

Drury, M. R. & Humphreys, F. J. 1986. The development of microstructure in Al15% Mg during high temperature deformation. *Acta metall.* **34**, 2259–2271

Drury, M. R. & Humphreys, F. J. 1987. Deformation lamellae as indicators of stress level (*Abstr.*). *Trans. Am. Geophys. Un.* (*EOS*) **68**, 1471.

Frost, H. J. & Ashby, M. F. 1982. *Deformation Mechanism Maps.* Pergamon Press, Oxford.

Heard, H. C. 1972. Steady-state flow in polycrystalline halite at pressure of 2 kilobars. In: *Flow and Fracture of Rocks. Geophys. Monogr.* **16**, 191–209.

Heard, H. C. & Carter, N. L. 1968. Experimentally induced 'natural' intragranular flow in quartz and quartzite. *Am. J. Sci.* **266**, 1–42.

Hori, H. & Nemat Nasser, S. 1985. Compression-induced microcrack growth in brittle solids: axial splitting and shear failure. *J. geophys. Res.* **90**, 3105–3125.

Jaoul, O., Tullis, J. & Kronenburg, A. 1984. The effect of varying water contents on the creep behaviour of Heavitree quartzite. *J. geophys. Res.***89**, 4298–4312.

Julivert, M. 1971. Decollement tectonics in the Hercynian Cordillera of N.W. Spain. *Am. J. Sci.***270**, 1–29.

Julivert, M. 1976. La Estructura der la region del Cabo-Peñas. *Trab. Geol. Univ. Oviedo* **8**, 203–309.

Julivert, M. & Arboleya, M. L. 1984. A geometrical and kinematical approach to the nappe structure in an arcuate fold belt: the Cantabrian Nappes (Hercynian chain, N.W. Spain). *J. Struct. Geol.* **6**, 499–519.

Julivert, M. & Arboleya, M. L. 1986. Areal balancing and estimate of areal reduction in thin-skinned fold-and-thrust belt (Cantabrian zone, N.W. Spain): constraints on its emplacement mechanism. *J. Struct. Geol.* **8**, 407–414.

Julivert, M. & Marcos, A. 1973. Superimposed folding under flexural conditions in the Cantabrian Zone (Hercynian Cordillera, N.W. Spain). *Am. J. Sci.* **273**, 353–375.

Koch, P. S. 1983. Rheology and microstructures of experimentally deformed quartz aggregates. Unpublished Ph.D. thesis, University of California, Los Angeles.

Koch, P. S. & Christie, J. M. 1981. Spacing of deformation lamellae as a palaeopiezometer (*Abstr.*). *Trans. Am. Geophys Un.* (*EOS*) **62**, 1030.

Koch, P. S., Christie, J. M. & George, R. P. 1980. Flow law of 'wet' quartzite in the α quartz field (*Abstr.*). *Trans. Am. Geophys. Un.* (*EOS*) **61**, 376.

Labuz, J. F., Shah, S. P. & Dowding, C. H. 1987. The fracture process zone in granite: evidence and effect. *Int. J. Rock Mech. Min. Sci. & Geomech. Abstr.* **24**, 235–246.

Lawn, B. R. & Wilshaw, T. R. 1975. *Fracture of Brittle Solids*. Cambridge University Press, Cambridge.

Marcos, A. 1979. Facies differentiation caused by wrench deformation along a deep seated fault system (Leon line, Cantabrian Mountains, North Spain)—Discussion. *Tectonophysics* **60**, 303–309.

Marcos, A. & Pulgar, J. A. 1982. An approach to the tectonostratigraphic evolution of the Cantabrian foreland thrust and fold belt, Hercynian cordillera of NW Spain. *Neues Jb. Geol. Paläont Abh.* **163**, 256–260.

McCormick, J. W. 1977. Transmission electron microscope investigation of some naturally deformed quartzites. Unpublished PhD. thesis, University of California, Los Angeles.

Nemat Nasser, S. & Hori, H. 1982. Compression-induced nonplanar crack extension with application to splitting, exfoliation, and rockburst. *J. geophys. Res.* **87**, 6805–6821.

Nix, W. D. & Ilscher, B. 1979. Mechanisms controlling creep of single phase metals and alloys. *Proc. 5th Conf. on Strength of Metals and Alloys*, 1503–1530.

Norton, M. G. 1982. The kinematic and microstructural development of some shear zones. Unpublished Ph.D. thesis, University of London.

Patterson, M. S. & Kekulawala, K. R. S. S. 1979. The role of water in quartz deformation. *Bull. Mineral.* **102**, 92–98.

Peck, L. 1983. Stress corrosion and crack propagation in Sioux quartzite. *J. geophys. Res.* **8**, 5037–5046.

Perroud, H. & Bonhommet, N. 1981. Palaeomagnetism of the Ibero-Armorican Arc and the Hercynian orogeny in Western Europe. *Nature, Lond.* **292**, 445–448.

Perroud, H., Van Der Voo, R. & Bonhommet, N. 1984. Palaeozoic evolution of the Armorica Plate on the basis of palaeomagnetic data. *Geology* **12**, 579–582.

Ries, A. C., Richardson, A. & Shackleton, R. M. 1980. Rotation of the Iberian Arc; palaeomagnetic results from North Spain. *Earth Planet. Sci. Lett.* **70**, 301–310.

Rudnicki, J. W. 1980. Fracture mechanics applied to the Earth's crust. *A. Rev. Earth Planet. Sci.* **8**, 489–525.

Schmidt, S. M., Boland, J. N. & Paterson, M. S. 1977. Superplastic flow in fine grained limestone. *Tectonophysics* **42**, 257–291.

Schmidt, S. M., Paterson, M. S. & Boland, J. N. 1980. High temperature flow and dynamic recrystallisation in Carrara marble. *Tectonophysics* **65**, 245-280.

Sherby, O. D. & Burke, P. M. 1968. Mechanical behaviour of crystalline solids at elevated temperature. *Prog. Mater. Sci.* **13**, 325–390.

Sibson, R. H., Moore, J. McM. & Rankin, A. H. 1975. Seismic pumping—a hydrothermal fluid transport mechanism. *J. geol. Soc. Lond.* **131**, 653.

Spiers, C. J., Urai, J. L., Lister, G. S., Boland, J. N. & Zwart, H. J. 1986. The influence of fluid rock interaction on the rheology of salt rock and on ionic transport in the salt. *Nuclear Science and Technology*, EUR 10399EN, Luxembourg.

Stel, M. 1981. Crystal growth in cataclasites: diagnostic microstructures and implications. *Tectonophysics* **78**, 585.

Swanson, P. L. 1981. Sub-critical crack propagation in Westerly granite: An investigation into the double torsion method. *Int. J. Rock Mech. Min. Sci. & Geomech. Abstr.* **18**, 445–449.

Tsenn, M. C. & Carter, N. L. 1987. Upper limits of power law creep of rocks. *Tectonophysics* **136**, 1–26.

Tullis, J., Christie, J. M. & Griggs, D. T. 1973. Microstructures and preferred orientations of experimentally deformed quartzites. *Bull. geol. Soc. Am.* **84**, 297–314.

Twiss, R. J. 1986. Variable sensitivity piezometric equations for dislocation density and subgrain diameter and their relevance to quartz and olivine. In: *Mineral and Rock Deformation: Laboratory Studies. Am. Geophys. Un. Geophys. Monogr.* **26**, 247–261.

White, S. H. 1973. Dislocation structures responsible for optical strain features in deformed quartz crystals. *J. Mater. Sci.* **8**, 490–499.

White, S. H., Drury, M. R., Ion, S. E. & Humphreys, F. J. 1985. Large strain deformation studies using magnesium as a rock analogue. Part 1: grain size palaeopiezometry in mylonite zones. *Phys. Earth & Planet. Interiors* **40**, 201–207.